Journal of Asian Concrete Federation
Vol. 4, No. 2, pp. 79-88, December 2018
ISSN 2465-7964 / eISSN 2465-7972
https://doi.org/10.18702/acf.2019.1.4.2.79
Copyright © Asian Concrete Federation. All rights reserved.

Technical Paper

Deformation mechanism of hardened cement paste under high stress and application of flow law

Yuya Sakai*

(Received: June 06, 2018; Accepted: November 02, 2018; Published online: January 04, 2019)

Abstract: In this study, a creep test was performed on hardened cement paste (HCP) with stepwise load increase at different confining pressures and saturation degrees. The strain rate–stress relationship, obtained under a stress of >75% of the maximum strength and plotted on a log–log chart, showed a slope of six. From previous studies on crystalline materials, such as rock, metal, and ice, it can be inferred that this slope indicates a deformation governed by dislocation creep. If dislocation creep occurs in HCP, the deformation may be governed by crystalline hydrates other than calcium silicate hydrate (C-S-H) because dislocation creep is generally not defined for gel materials. Further study and careful discussion are required because a slope of six is a necessary condition for the dislocation creep. The activation volume was evaluated, and the flow law was applied to calculate the strain rate of HCP. The obtained activation volume gives a better fit for the measured results than the previously reported values.

Keywords: cement paste, triaxial test, flow law, dislocation creep.

1. Introduction

Concrete is one of the most important construction materials in the world and has been used for a long time. However, the mechanism of concrete deformation has not yet been fully understood. For example, creep deformation was reported more than 100 years ago [1], but its mechanism is still a subject of discussion. The main mechanisms of creep deformation proposed so far are based on microcrack formation [2], water seepage from hardened cement paste (HCP) [3], occurrence of slip between the globules of calcium silicate hydrate (C-S-H) [4], occurrence of microprestress [5], etc. Gaining a clear understanding of the concrete deformation mechanism is important for the safe and rational design and maintenance of concrete structures. With regard to creep deformation, it is known that the stress higher than the threshold stress causes creep fracture, and this threshold stress is called the sustained load strength [6–8]. The sustained load strength usually ranges from 70% to 80% of the maximum strength in normal concrete [6,9,10], although higher fractions (e.g. > 85%) have been reported for high-strength concrete [11,12]. Hsu et al. [13] studied the development of cracks in concrete and reported that matrix cracks formed continuous crack patterns under a stress of more than 70% of the maximum strength. Because this fraction (percentage of the sustained load strength in relation to the maximum strength) agrees with the ratio of the applied stress to the maximum strength, crack development may be related to the sustained load strength; however, the origin of the sustained load strength has not yet been clearly explained. The ratio between the sustained load strength and maximum strength for various types of concrete is almost consistent, which indicates that they have a common mechanism; gaining an understanding of the deformation mechanism under high stress (stress higher than the sustained load strength) may lead to a better understanding of the failure mechanism of concrete.

In this study, the deformation mechanism of HCP was studied by performing triaxial tests. The results showed that a shear plane was not formed in HCP that was subjected to a certain confining pressure, even though the HCP deformed upon the application of up to 10% strain [14]. Based on this result, it was inferred that the HCP shows plastic flow when subjected to a certain confining pressure. The plastic flow of HCP was clearly observed during the compaction of crushed HCP [15]. The mechanism of the flow was studied by performing a creep test with a stepwise increase in the load. Furthermore, the strain rate was calculated assuming that the HCP reached a static state within 20 min after the load increase [14].

Corresponding author Yuya Sakai is an Assistant Professor of Institute of Industrial Science, The University of Tokyo, Tokyo, Japan.

However, this assumption was not appropriate because HCP requires a longer time to reach a static state under sustained load [6]. The obtained results were not consistent and not easy to analyze or interpret. Moreover, a model to describe the deformation of HCP was not proposed. The strain rate due to plastic deformation is described by the flow law that is often applied to inorganic materials, such as rocks, ceramics and metals [16,17]. However, to the best of our knowledge, the application of the flow law to HCP has not been studied yet.

Therefore, in this study, another analysis method was applied to the results of the stepwise creep test, additional experiments were performed to apply the flow law, and a quantitative discussion was included on the deformation mechanism of HCP. First, a loading test was performed at a constant strain rate to obtain the maximum strength. The samples were cut after the test and the cross-sectional surfaces were observed. Subsequently, a creep test was performed with a stepwise increase in the load corresponding to 30–95% of the maximum strength. The deformation mechanism of the HCP was discussed based on the obtained strain rate–stress relationship. The activation volume was evaluated, and the flow law was applied to describe the deformation of the HCP under high stress.

2. Methodology

2.1 Sample preparation

In this research, cement paste (water-to-cement ratio = 0.4) made from ordinary Portland cement was used. The properties of the cement are presented in Tables 1 and 2. The mixing procedure was based on JIS R 5201. The paste was first mixed for 60 seconds in a mixer operating at a low speed (orbital rotation: 62 ± 5 rpm, planetary rotation: 140 ± 5 rpm). The mixer was stopped for 30–60 seconds to scrape off cement paste on the sides of the mixing bowl and paddle. Then, the paste was mixed for 90 seconds at a high speed (orbital rotation: 125 ± 5 rpm, planetary rotation: 285 ± 5 rpm). The mixed paste was cast in a plastic mould (250 × 150 × 100 mm) and sealed. It was demoulded 24 hours after casting and then kept under water for two months. The temperature of the room and water was 24 °C. After curing, cylinders of φ10 mm were cored from the HCP mass. Only the part deeper than 2 cm from the surface was used. Both ends of the cylinder were ground to achieve flat and parallel surfaces. The prepared cylinders (φ10 × 24 mm) were immersed into acetone for 24 hours to stop the hydration reaction and reduce capillary suction in the subsequent drying period. After immersion, the cylinders were dried in a desiccator at 24 °C and 20% RH until the weight change over 24 hours because of moisture loss was less than 0.1% of the specimen weight. Saturated samples were prepared by immersing the cylinders into tap water after drying at 24 °C and 20% RH until the weight change over 24 hours was less than 1% of the specimen weight. The specimen names are composed of the alphabets D or W followed by numbers (e.g. D0, W50); D and W indicate dry and saturated samples, respectively, and the number indicates the confining pressure P_c. Assuming that the saturation degrees of the saturated and oven-dried (at 105 °C) samples were unity and 0, respectively, the calculated saturation degree of a sample dried at 24 °C and 20% RH was 0.31. Considering that HCP was immersed in acetone, this saturation degree (0.31) was a mixture of water and acetone. The testing age varied in the range of 5–6 months. The carbonation depth of the sample, which was kept in the desiccator (24 °C and 20% RH) after all tests, was measured using a 1% solution of phenolphthalein in ethyl alcohol. The sample was split horizontally at the middle using a chisel, and the solution applied on the fracture surface indicated that the sample had a carbonation depth of 0.5 mm. The porosity of the sample, which was calculated using the following equation, was found to be 0.39.

$$\phi = 1 - (W_{oven} - W_{water})/(W_{sat} - W_{water}) \quad (1)$$

where φ is the porosity, W_{oven} is the oven-dried weight, W_{water} is the saturated weight under water, and W_{sat} is the saturated weight in the air.

Table 1 – Chemical composition of cement

Chemical property (%)									
Ig. loss	Insol.	SiO_2	Al_2O_3	Fe_2O_3	CaO	MgO	SO_3	Na_2O	K_2O
2.84	0.27	19.83	4.56	2.95	61.28	3.78	2.83	0.35	0.57

Table 2 – Physical properties of cement

Density (g/cm^3)	Specific surface area (cm^2/g)
3.12	4,110

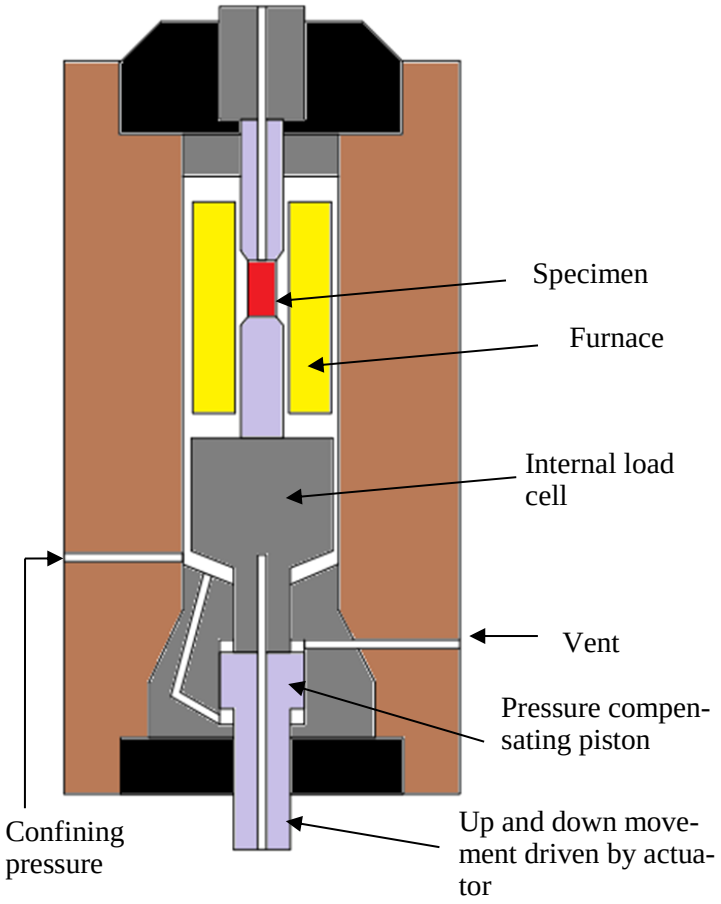

Fig. 1 − Schematic diagram of triaxial testing apparatus

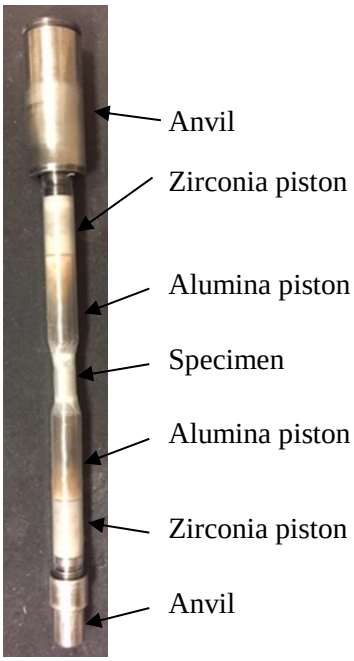

Fig. 2 − Sample assembly

2.2 Triaxial test

2.2.1 Test apparatus and sample assembly

The Paterson-type [18] triaxial test apparatus was used with argon gas as the pressure medium to generate confining pressure on the sample. The schematic view of the apparatus is shown in Fig. 1. A sample was placed between alumina and zirconia pistons enclosed in a heat-shrinkable (polyolefin) tube that sealed the sample from the confining medium. The end face of the HCP sample was exposed to the laboratory atmosphere through small centre holes in the spacers and pistons to avoid pore pressure being generated during experiments. To achieve shrinkage, the tube was heated from the outside using a heat gun. To check the temperature of the HCP specimen during the heat treatment on the tube, a 2-mm-diameter hole was created on the HCP sample and the temperature in the hole was measured using a needle probe thermometer [19]. The distance from the sample surface to the hole was 2 mm. A heat-shrinkable tube was placed over the HCP sample and heated until the tube touched the sample completely. The maximum temperature reached was 46 °C; therefore, the heat might have some effect near the surface of the sample during this heating process. A saturated sample was wrapped with a plastic film before being covered with a heat-shrinkable tube. Steel anvils were then attached to the top and bottom of the zirconia pistons and fixed with steel wires over the heat-shrinkable tube. Figure 2 shows a photograph of the sample assembly. The prepared sample assembly was inserted into the pressure vessel of the test apparatus. Load was applied by moving the lower piston upward. The stress was calculated by dividing the load measured using the internal load cell by the cross-sectional area of the sample. The apparatus was designed such that the confining pressure did not affect the stress measured by the internal load cell; therefore, the calculated stress corresponded to the differential stress. The axial strain was calculated by dividing the displacement measured using the transducer located below the sample assembly by the initial length of the sample. The load, displacement, and confining pressure were measured at intervals of 1 second. All the tests were performed at room temperature (24 °C).

2.2.2 Constant strain rate loading test

Triaxial tests with constant strain rate loading were performed at 1.4×10^{-4} s^{-1}. Two dry samples were tested at each value of P_c; one of the two samples was loaded until the strain reached 10%, and the

other one was loaded until the stress started decreasing after reaching the maximum stress (σ_{max}). Samples tested at P_c = 0 MPa were loaded until the stress decrease stagnated.

After the triaxial tests with constant strain rate loading, the sample covered with a heat-shrinkable tube was cut out from the assembly and impregnated into a two-component epoxy resin (room-temperature curing). The sample was then cut parallel to the long axis when the epoxy resin hardened. The cutting surface was polished using alumina powder (average diameter = 55 and 15 μm) and observed by the naked eye.

2.2.3 Stepwise creep test

A stepwise creep test was performed to obtain strain rate–stress relationship. In this test, the applied stress was increased stepwise from 30% to 95% of σ_{max}. The stress was increased every 30–60 minutes. The strain rate–stress relationship is known to show more internal consistency in the stepwise creep test than in the conventional creep test [20, 21]. In a previous study, the strain rate was calculated when the slope of the strain–time curve was regarded to be in a static state, but the slope actually kept decreasing and did not reach a static state [14]. Thus, as in the study by Zhang and Spiers [22], who studied the compaction mechanism of calcite powder, the strain rates were calculated from the slope of the strain increment-time relationship at certain strain values. The strain rate of D0 was calculated using data obtained 1000–2000 seconds after each value of stress was attained, and that of W0 was obtained by fitting the exponential approximate function for the entire data set because the strain in the samples without P_c was small. The strain rate at steady-state creep is described by the following flow law [23]:

$$\dot{\varepsilon} = A\sigma^n d^{-m} \exp\{-(Q+PV)/RT\} \quad (2)$$

where $\dot{\varepsilon}$ is the strain rate (s^{-1}), A is a constant (m^m/Pa^n), σ is the differential stress (Pa), n is the stress exponent, d is the grain size (m), m is the grain size exponent, Q is the activation energy (J/mol), P is the pressure (Pa), V is the activation volume (m^3/mol), R is the gas constant (= 8.3 J/K/mol), and T is the absolute temperature (K). The slope of the strain rate-stress relationship corresponds to n.

2.3 Hydrostatic pressure test

The value of the activation volume is necessary for applying the flow law to the deformation of HCP. The equation to calculate the activation volume is derived from Eq. (2) by taking the natural logarithm and differentiating partially with respect to P (assuming σ to be a constant) as follows:

$$\ln \dot{\varepsilon} = \ln A + \ln \sigma - m \ln d - Q/RT - PV/RT \quad (3)$$

$$\partial \ln \dot{\varepsilon}/\partial P = -V/RT \quad (\sigma\text{: constant}) \quad (4)$$

$$V = -RT\partial \ln \dot{\varepsilon}/\partial P \quad (5)$$

To calculate V using Eq. (5), it is necessary to determine $\dot{\varepsilon}$ for different P (P_c) values with σ being constant. However, as shown later in Section 3.2, the strain rate–stress relationship follows the flow law only when σ is more than 75% of σ_{max}. Because σ_{max} of dry samples increases with an increase in P_c, the constant σ can be less than 75% of σ_{max} with increasing P_c and V would be calculated in the region where the data do not follow the flow law. Therefore, V was calculated by measuring the strain rate of a saturated sample for different P_c values with a constant σ (92 MPa, 80% of σ_{max} in W20) because σ_{max} of the saturated sample hardly depends on P_c, as shown later in Section 3.1. For the saturated sample, P_c was first set to 20 MPa, σ corresponding to 80% of σ_{max} was applied, and P_c was then increased by 10 MPa up to 50 MPa to obtain the ln $\dot{\varepsilon}$–P_c relationship.

3. Results

3.1 Constant strain rate loading test

The differential stress–strain curves of the dry samples are shown in Fig. 3(a). The results for the samples loaded until ε = 10% and those loaded until the stress started decreasing are represented by broken lines and solid lines, respectively. The two samples with the same P_c showed similar results. D0 showed a sudden stress decrease after σ_{max}. σ_{max} increased with an increase in P_c. The stress kept increasing until ε = 10% for P_c = 100 MPa, but the stiffness decreased in the low-strain region. Figure 3(b) shows the results for the saturated samples. Compared to the dry samples tested at the same P_c, σ_{max} for the saturated samples decreased. W20 and W50 showed similar curves.

Figure 4 shows the cut and polished surfaces of the samples after the triaxial tests. Except for D0, the left image shows the sample loaded up to 10% strain and the right image shows the sample loaded until the stress started decreasing. D30 shows only the sample loaded up to 10% strain. The black lines in the samples are the epoxy resin that penetrated through the cracks. Vertical cracks developed in D0, and shear planes were formed in D10, D30, and D50. A shear plane was not formed in D100.

3.2 Stepwise creep test

The obtained strain increment–time curves are shown in Fig. 5. The values in the legends indicate stress (the values in parentheses indicates the ratio of

the applied stress to σ_{max}). The values in parentheses at the upper right corner are the strain values at which $\dot{\varepsilon}$ was calculated. Figure 6 shows the relationship between $\dot{\varepsilon}$ and σ, with the lines indicating slopes of three and six. The data for stress values less than 0.75 × σ_{max} are shown as plots represented by short lines, and the data for stress values equal to or greater than 0.75 × σ_{max} are shown as plots represented by circles. The plots represented by the short lines are scattered, whereas the plots represented by the circles are distributed linearly, except for D0, and have slopes close to six.

3.3 Hydrostatic pressure test

Figure 7 shows the strain–time relationship and ln $\dot{\varepsilon}$–P_c relationship of a saturated sample in the hydrostatic pressure test. According to Eq. (5), the slope of the plots in Fig. 7(b), -3×10^{-8}, multiplied by -RT is equal to V, and the calculated V for the saturated samples was 7.4×10^{-5} m^3/mol.

4. Discussion

4.1 Deformation mechanism of HCP under high stress

The dry samples showed stress decrements, and vertical cracks or shear planes were formed when P_c was 0–50 MPa. When P_c was 100 MPa, the stress increased up to 10% strain and no shear plane was formed. In rock mechanics, fractures at lower strains with vertical cracks or shear planes are considered brittle, whereas those at higher strains without shear planes are considered ductile [18]. Following this classification, the HCP deformation changed from brittle to ductile with an increase in P_c. These results are consistent with those obtained in a previous study [14]. The horizontal crack in the sample shown on the right side of Fig. 4(d) might have been formed during unloading.

As seen in Fig. 3(a), the stress did not decrease when P_c was 100 MPa; a similar tendency has been reported for concrete [24]. However, HCP showed a decrease in stress in the low-strain region, whereas concrete did not. A possible reason for this difference is that the aggregate and concrete were in contact with each other. Consequently, the aggregate generated resistance that prevented a decrease in stress. In porous rocks, stress decreases due to microscopic damage has been reported [25,26], and a similar phenomenon might have occurred in HCP. In Figure 6, the strain rate–stress relationship at stress values greater than 0.75 × σ_{max} is seen to be distributed linearly and the slope is approximately six. This slope corresponds to n in Eq. (2).

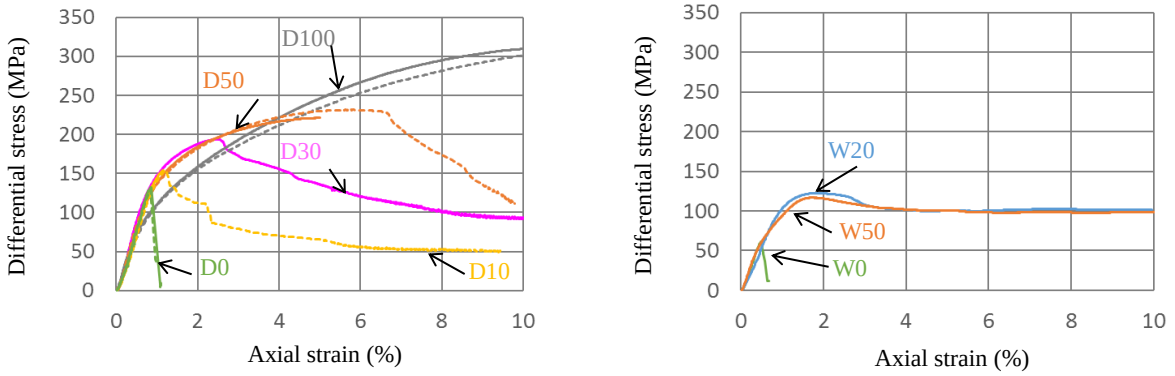

(a) Dry specimens (b) Saturated specimens

Fig. 3 − Differential stress–axial strain relationship with constant strain rate loading

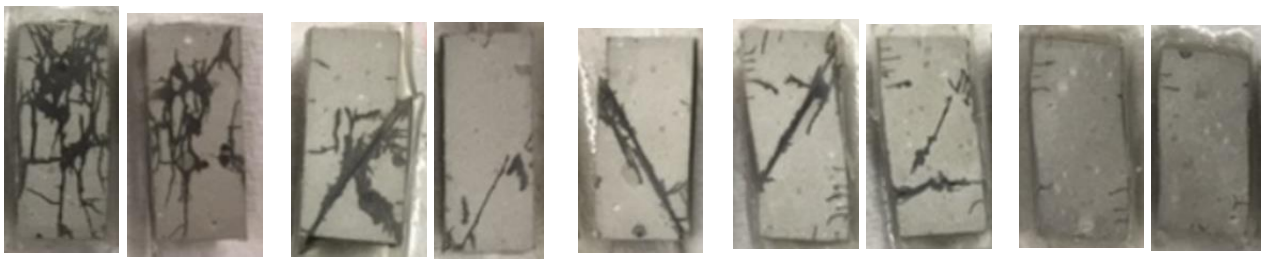

(a) D0 (b) D10 (c) D30 (d) D50 (e) D100

Fig. 4 − Cross section of dry specimens after constant strain rate loading test

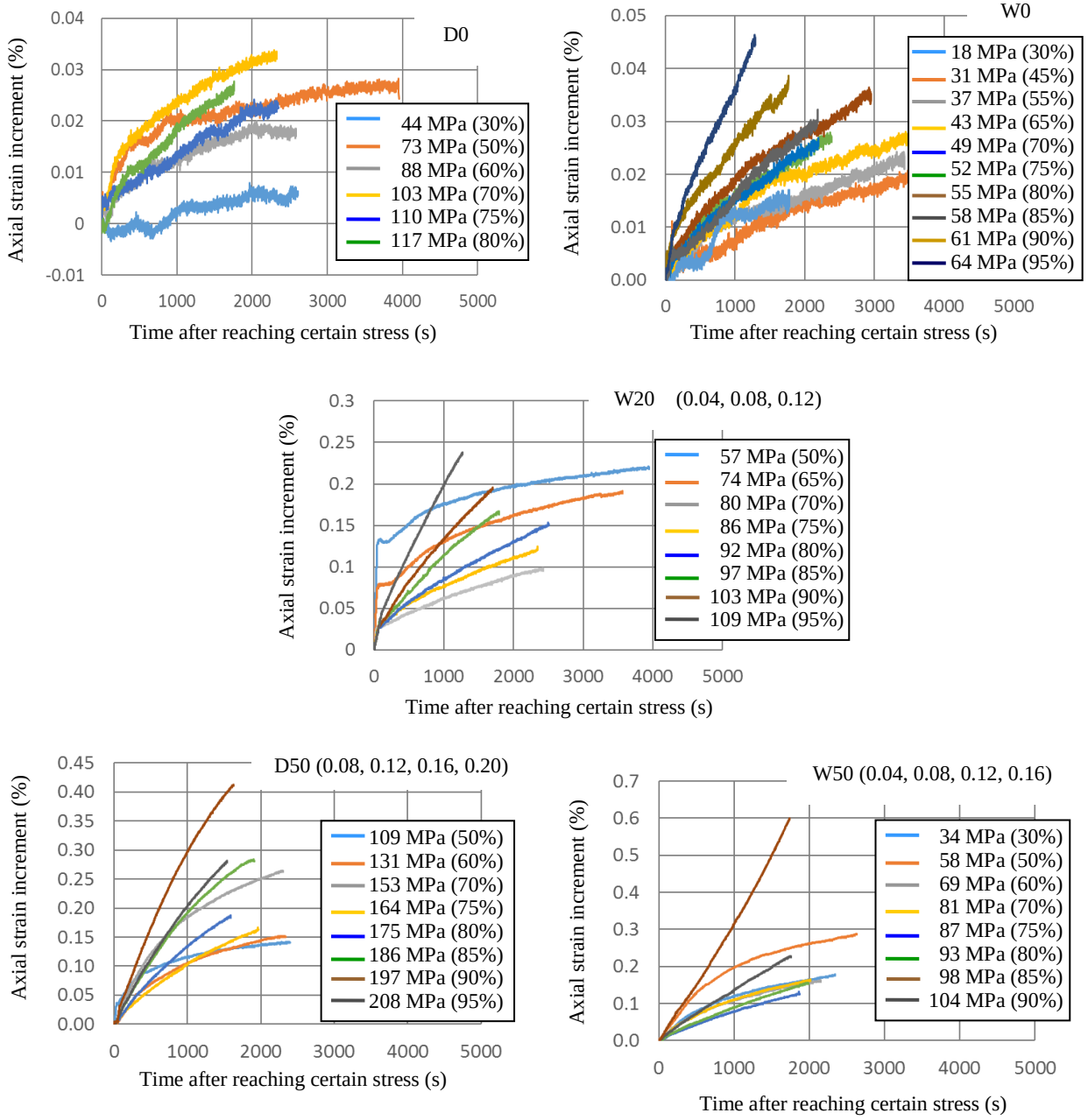

Fig. 5 − Strain increment–time relationship in stepwise creep test

The creep mechanisms of crystalline materials are classified according to the value of n: $n = 1$ is considered to represent diffusion creep (creep deformation governed by atomic diffusion), and $n > 1$ is considered to represent dislocation creep (creep deformation governed by dislocation movement) [26,27]. Bürgmann and Dresen [28] classified $n = 3$–6 as creep governed by dislocation climb. Various crystalline materials such as metal [29] and ice [30] have similar equations and classifications. Thus, the slope of six seen in Fig. 6 indicates that the deformation of HCP for stress values larger than $0.75 \times \sigma_{max}$ is governed by dislocation climb. The same slopes for the dry and saturated samples indicate that the deformation mechanism does not change according to the saturation degree. Concrete generally fails when it is subjected to a stress larger than a sustained load strength that is approximately 75% of the maximum strength [6,9,10]. This fraction corresponds to the threshold stress above which data are distributed with the slope of six in Fig. 6. This correspondence indicates that the creep failure in concrete may be attributed to deformation due to dislocation creep. Many materials show plastic deformation, which is sometimes followed by brittle fracture. In addition, the interaction between cracks and dislocation plays an important role in plastic deformation [31]. Therefore, the propagation of cracks in HCP at stress values of more than 70% of the maximum strength may be affected by dislocations. However, it should be noted that the slope of six is a necessary, but not sufficient, condition for dislocation creep.

4.2 Application of flow law

The flow law (Eq. (2)) was applied to the obtained results. Figure 6 shows the results for $n = 6$ and $m = 0$ for the dislocation creep. The value of Q was set as 35,000 J/mol [39,32] for the dry sample and 17,500 J/mol for the saturated sample [31–33] based on the results for rocks. The obtained V for the saturated sample was 7.4×10^{-5} m^3/mol. Sammis et al. [36] reported the Q and V values for various materials; the values obtained in this study were close to those of the ionic crystals. The value of V for the dry sample was also assumed to be 7.4×10^{-5} m^3/mol because a similar value was previously reported for dry and wet rocks [33–35]. The value of V reported by Klug and Wittmann [37] was 1×10^{-20} cm^3 (6×10^{-3} m^3/mol), which was approximately 100 times larger than the one obtained in this study. For fitting the calculation results to the measured data, A was set to 1×10^{-23} for the dry samples and 5×10^{-15} for the saturated samples. The calculated curves using these parameters are shown in Fig. 8(a) along with the measured data for stress values larger than $0.75 \times \sigma_{max}$; the calculated and measured data are in good agreement. Figure 8(b) shows the calculated curves obtained using the value of V reported by Klug and Wittmann [37]. The value of A was adjusted to obtain the best possible fit for the data ($A = 1 \times 10^{15}$ for dry and saturated samples) but the calculated curves varied significantly depending on P_c and deviated from the measured data. In Equation (2), V expresses the dependency of $\dot{\varepsilon}$ on P_c; therefore, the value of V reported by Klug and Wittmann [37] is likely to be too large to describe the deformation of HCP under high stress based on the flow law.

4.3 Contribution of C-S-H to deformation of HCP

The strain rate–stress relationship of HCP in Fig. 6 indicates that the deformation of HCP was governed by dislocation similar to the case of crystalline materials such as rock [27,28], metal [29], and ice [30]. In concrete, dislocation was reported to occur in calcium hydroxide because of the stress caused by drying shrinkage [38]. However, 50–60% of the HCP volume is composed of C-S-H, which is generally regarded as a gel. Klug [39] and Klug and Wittmann [37] discussed the creep deformation of HCP, assuming the deformation of the amorphous solid skeleton. However, the plastic deformation mechanism of an amorphous material, such as metallic glass, is explained by the shear band formation or local atomic jump [41,42]. In both these mechanisms, the strain rate is a hyperbolic function of stress, and the value of n changes from 1 to a very large number. The consistent slope of six obtained in this study indicates that the deformation mechanism of HCP is closer to that of a crystalline material than an amorphous material. The time-dependent response of C-S-H has been studied using various approaches, and recently, atomistic simulation has appeared as a powerful tool for its investigation. Morshedifard et al. [40] carried out a molecular dynamics simulation to study the time-dependent response of C-S-H, and they reported a behavior often seen in glassy systems. In addition, these authors reported that the amount of interlayer water changes the time-dependent response of C-S-H. If the response of C-S-H under high stress is similar to metal glass and if dislocation creep occurs in HCP, crystalline hydrates such as calcium hydrates or ettringite may govern the deformation under high stress. As these crystalline hydrates are not dominant in volume, they likely form a skeleton to resist the applied load, and the deformation of this structure may be governed by the dislocation creep [43]. The calcium hydroxide crystal is large, and its aspect ratio is high. Generally, to form a skeleton, the element volume fraction needs to be more than about 16% [44,45]. However, when the aspect ratio is high, the required volume fraction decreases significantly [46,47], and a skeleton is formed more easily. The volume fraction of the hydrates other than C-S-H is around 40%, which is sufficiently large for the hydrates to form a structure. Further study is necessary to conclude the deformation mechanism.

5. Conclusion

In this study, a stepwise creep test was performed to understand the deformation mechanism of hardened cement paste. Subsequently, the flow law was applied to the obtained test results. The following conclusions were derived:

(1) The maximum strength of the saturated samples was lower than that of the dry samples under any given confining pressure.

(2) The strain rate and differential stress relationship obtained in the creep test with a stepwise increase in the load showed a slope of six on a log–log chart. This slope indicates that the deformation is governed by dislocation creep.

(3) Dislocation creep might have possibly caused the fracture of concrete when the stress was larger than the sustained load strength.

(4) The calculated strain rate based on the flow law showed that the obtained activation volume was reasonable whereas the one reported by a previous study was too large.

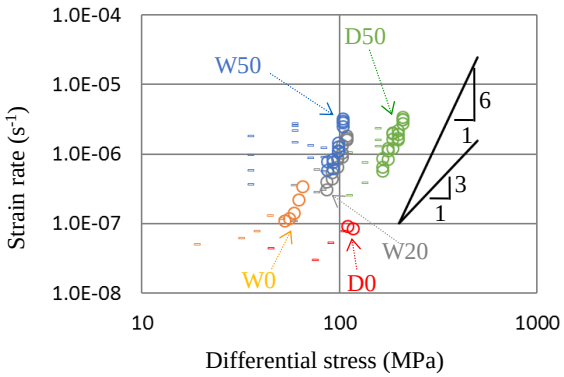

Fig. 6 − Strain rate–differential stress relationship in stepwise creep test

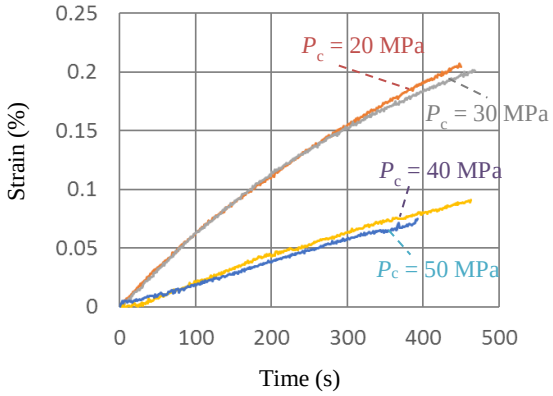

(a) Strain–time relationship

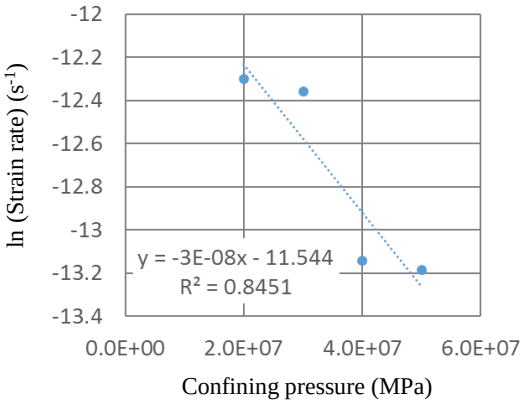

(b) Strain rate–confining pressure relationship

Fig. 7 − Strain–time and strain rate–confining pressure relationships in hydrostatic pressure

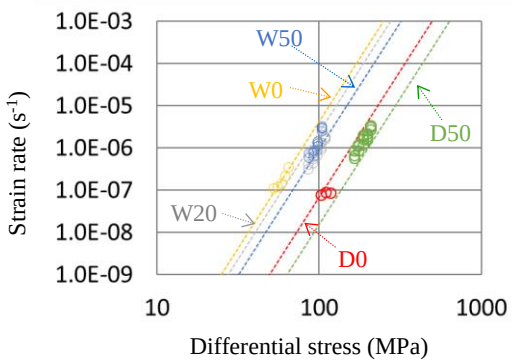

(a) $V = 7.4 \times 10^{-5}$ m^3/mol

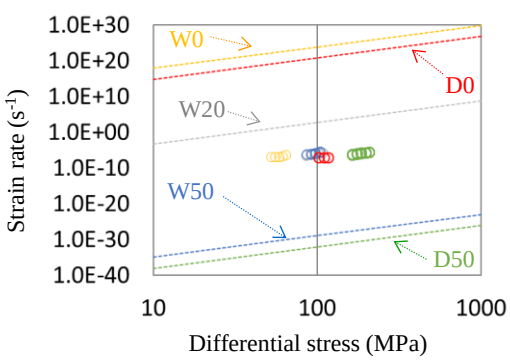

(b) $V = 6 \times 10^{-3}$ m^3/mol

Fig. 8 − Strain rate–differential stress relationship in stepwise creep test along with calculated strain rate based on flow law

(5) Because 50–60% of the cement paste volume is composed of the gel hydrate C-S-H, dislocation cannot be defined in a gel. Other crystalline hydrates could likely govern the deformation, similar to the deformation governed by dislocation creep.

The results of this study indicate that dislocation might play an important role in the deformation of hardened cement pastes under high stress. If this is true, dislocation may govern various failure patterns of concrete, such as fatigue. Further study and careful discussion in this regard are necessary because the slope of six in the strain rate–stress relationship is a necessary but not a sufficient condition for dislocation creep.

Acknowledgements

This study was supported by the Foundation for the Promotion of Industrial Science, Tokyo, Japan. The triaxial tests in this study was performed using the apparatus owned by the Department of Earth, Environmental, and Planetary Science, Brown University, Rhode Island, USA.

References

1. Hatt, W.K. (1907) "Notes on the effect of time element in loading reinforced concrete beams," Proceedings ASTM, 7, pp. 421~433.
2. Pickett, G. (1942) "The effect of change in moisture content on the creep of concrete under a sustained load," Journal of American Concrete Institute, 38, pp. 333~355.
3. Powers, T.C. (1968) "The thermodynamics of volume change and creep," Matériaux et Construction, 1(6), pp. 487~507.
4. Ali, I. and Kesler, C. (1964) "Mechanisms of creep in concrete," Symposium on Creep of Concrete, Detroit, ACI Publication SP-9, pp. 35~63.
5. Bažant, Z.P.; Hauggaard, A.B.; Baweja, S.; and Ulm, F.J. (1997) "Microprestress-solidification theory for concrete creep. I: Aging and drying effects," Journal of Engineering Mechanics, 123(11), pp. 1188~1194.
6. Rüsch, H. (1960) "Researches toward a general flexural theory for structural concrete," Journal of American Concrete Institute, 57(1), pp. 1~28.
7. Carpinteri, A.; Valente, S.; Zhou, F.P.; Ferrara, G.; and Melchiorri, G. (1997) "Tensile and flexural creep rupture tests on partially damaged concrete specimens," Materials and Structures, 30(5), pp. 269~276.
8. Ranaivomanana, N.; Multon, S.; and Turatsinze, A. (2013) "Tensile, compressive and flexural basic creep of concrete at different stress levels," Cement and Concrete Research, 52, pp. 1~10.
9. Ngab, A.S.; Nilson, A.H.; and Slate, F.O. (1981) "Shrinkage and creep of high strength concrete," Journal of American Concrete Institute, 78(4), pp. 255~261.
10. Smadi, M.M.; Slate, F.O.; and Nilson, A.H. (1982) "Time-dependent behavior of high-strength concrete under high sustained compressive stresses," Research Report No. 82 –16, Department of Structural Engineering, Cornell University, Ithaca, NY.
11. Smadi, M.M.; Slate, F.O.; and Nilson, A.H. (1985) "High-, medium-, and low-strength concretes subject to sustained overloads-strains, strengths, and failure mechanisms," Journal of American Concrete Institute, 82(5), pp. 657~664.
12. Iravani, S. and MacGregor, J.G. (1994) "High performance concrete under high sustained compressive stresses," Structural Engineering Report No. 200, Department of Civil Engineering, University of Alberta.
13. Hsu, T.T.C; Slate, F.O.; Sturman, G.M.; and Winter, G. (1963) "Microcracking of plain concrete and the shape of the stress-strain curve," Journal of American Concrete Institute, 60(2), pp. 209~224.
14. Sakai, Y and Kishi, T. (2017) "Deformation mechanism of hardened cement paste and effect of water," Journal of Advanced Concrete Technology, 15(1), pp. 19~28.
15. Sakai, Y.; Tarekegne, B.T.; and Kishi, T. (2016) "Recycling of hardened cementitious material by pressure and control of volumetric change," Journal of Advanced Concrete Technology, 14(2), pp. 47~54.
16. Goetze, C. (1978) "The mechanisms of creep in olivine," Philosophical Transactions of the Royal Society of London. Series A, Mathematical and Physical, 288(1350), pp.99-119.
17. Frost, H.J. and Ashby, M.F. (1982) "Deformation-mechanism Maps: The Plasticity and Creep of Metals and Ceramics," Pergamon Press.
18. Paterson, M. and Wong, T. (2005) "Experimental Rock Deformation - The Brittle Field," Springer Science & Business Media, Berlin.
19. Sakai, Y.; Nakatani, M.; Takeuchi, A.; Omorai, Y.; and Kishi, T. (2016) "Mechanical behavior of cement paste and alterations of hydrates under high-pressure triaxial testing," Journal of Advanced Concrete Technology, 14(1), pp. 1~12.
20. Heap, M.J.; Baud, P.; Meredith, P.G.; Bell, A.F.; and Main, I.G. (2009) "Time-dependent brittle creep in Darley Dale sandstone," Journal of Geophysical Research: Solid Earth, 114, B07203.
21. Brantut, N.; Heap, M.J.; Meredith, P.G.; and Baud, P. (2013) "Time-dependent cracking and brittle creep in crustal rocks: A review," Journal of Structural Geology, 52, pp. 17~43.
22. Zhang, X. and Spiers, C.J. (2005) "Compaction of granular calcite by pressure solution at room temperature and effects of pore fluid chemistry," International Journal of Rock Mechanics and Mining Sciences, 42, pp. 950~960.
23. Jackson, I. (2000) "The Earth's Mantle: Composition, Structure, and Evolution," Cambridge University Press, Cambridge.
24. Sfer, D.; Carol, I.; Gettu, R.; and Etse, G. (2002) "Study of the behavior of concrete under triaxial compression," Journal of Engineering Mechanics, 128(2), pp. 156~163.

25. Lubarda, V.A.; Mastilovic, S.; and Knap, J. (1996) "Brittle-ductile transition in porous rocks by cap model," Journal of Engineering Mechanics, 122(7), pp. 633~642.
26. Zheng, Z.; McLennan, J.D.; and Martin, J.W. (1991) "Compressive stress-induced microcracks and effective elastic properties of limestone and concrete," Final Technical Report to USAF, Topic No. AF90-186, Terra Tek Report TR91-107.
27. Mei, S. and Kohlstedt, D.L. (2000) "Influence of water on plastic deformation of olivine aggregates: 2. Dislocation creep regime," Journal of Geophysical Research, 105(B9), pp. 21471~21481.
28. Bürgmann, R. and Dresen, G. (2008) "Rheology of the lower crust and upper mantle: Evidence from rock mechanics, geodesy, and field observations," Annual Review of Earth and Planetary Sciences, 36, pp. 531~567.
29. Sato, E.; Yamada, T.; Tanaka H.; and Jimbo, I. (2005) "Categorization of ambient temperature creep behavior of metals and alloys on their crystallographic structures," Journal of Japan Institute of Light Metals, 55(11), pp. 604~609.
30. Goldsby, D.L. and Kohlstedt, D.L. (1995) "The transition from dislocation to diffusion creep in ice," Abstracts of the Lunar and Planetary Science Conference, 26, pp. 473~474.
31. Ohr, S.M. (1987) "Dislocation-crack interaction," Journal of Physics and Chemistry of Solids, 48(11), pp. 1007~1014.
32. Riding, K.A. and Siddiqui, S. (2012) "Effect of calculation methods on cement paste and mortar apparent activation energy," Advances in Civil Engineering Materials, 1(1), pp. 1~19.
33. Karato, S.I. and Wu, P. (1993) "Rheology of the upper mantle: A synthesis," Science, 260(5109), pp. 771~778.
34. Karato, S.I. and Jung, H. (2003) "Effects of pressure on high-temperature dislocation creep in olivine," Philosophical Magazine, 83(3), pp. 401~414.
35. Rybacki, E.; Gottschalk, M.; Wirth, R.; and Dresen, G. (2006) "Influence of water fugacity and activation volume on the flow properties of fine-grained anorthite aggregates," Journal of Geophysical Research: Solid Earth, 111(B3), B03203.
36. Sammis, C.G.; Smith, J.C.; and Schubert, G. (1981) "A critical assessment of estimation methods for activation volume," Journal of Geophysical Research: Solid Earth, 86(B11), pp. 10707~10718.
37. Klug, P. and Wittmann, F. (1974) "Activation energy and activation volume of creep of hardened cement paste," Materials Science and Engineering, 15(1), pp. 63~66.
38. Harutyunyan, V.S.; Abovyan, E.S.; and Monteiro, P.J.M. (2003) "X-ray diffraction investigations of deformations and dislocation con-Figureuration in calcium hydroxide crystallites of concrete," Physica Status Solidi, 200(2), pp. 307~325.
39. Klug, P. (1969) "Activation energy of creep of hardened cement paste," Matériaux et Construction, 2(1), pp. 11~16.
40. Morshedifard, A.; Masoumi, S.; and Abdolhosseini Qomi, M.J. (2018) "Nanoscale origins of creep in calcium silicate hydrates," Nature Communications, 9, 1785.
41. Schuh, C.A.; Hufnagel, T.C.; and Ramamurty, U. (2007) "Mechanical behavior of amorphous alloys," Acta Material, 55(12), pp. 4067~4109.
42. Kassner, M.E.; Smith, K.; and Eliasson, V. (2015) "Creep in amorphous metals," Journal of Materials Research and Technology, 4(1), pp. 100~107.
43. Sakai, Y. and Uehara, Y. (2018) "Deformation mechanism of cement paste and hydrates under high stress," Journal of Advanced Concrete Technology, 16(6), pp. 262~271.
44. Scher, H. and Zallen, R. (1970) "Critical Density in Percolation Processes," The Journal of Chemical Physics, 53(9), pp. 3759~3761.
45. Bentz, D.P. and Garboczi, E.J. (1991) "Percolation of phases in a three-dimensional cement paste microstructural model," Cement and Concrete Research, 21(2), pp. 325~344.
46. Garboczi, E.J.; Snyder, K.A.; Douglas, J.F.; and Thorpe, M.F. (1995) "Geometrical percolation threshold of overlapping ellipsoids," Physical Review E, 52(1), pp. 819~828.
47. Saar, M.O. and Manga, M. (2002) "Continuum percolation for randomly oriented soft-core prisms," Physical Review E, 65(5), 056131.